J Mater Sci (2008) 43:7066–7072
DOI 10.1007/s10853-008-3056-5

Characterization and reactivity of chromia nanoparticles prepared by urea forced hydrolysis

Heather J. Gulley-Stahl · Whitney L. Schmidt · Heather A. Bullen

Received: 21 July 2008 / Accepted: 15 October 2008 / Published online: 30 October 2008

Abstract Chromia (Cr_2O_3) nanoparticles were prepared by urea forced hydrolysis in the presence of chromium (III) nitrate using NaCl as a precipitating agent. The size, distribution, and purity of the particles were evaluated. The necessity of polyvinylpyrrolidone (PVP) as a surfactant to prevent aggregation was also investigated. In the presence of PVP, non-aggregated spherical-like nanoparticles (3 ± 1 nm) were formed, whereas in the absence of PVP, spherical-like weakly agglomerated nanoparticles (85 ± 16 nm) comprised of 10 nm nanoparticle subunits were produced, creating a large surface area. The as-formed hydrated Cr_2O_3 nanoparticles were amorphous, although they could be easily converted into crystalline form by heating to 400 °C for 1 h, with minimal particle aggregation and size reduction. Attenuated total reflectance Fourier transform infrared spectroscopy indicated that preparation methods (surfactant and precipitating agent) influence surface reactivity of the nanoparticles to catechol.

Introduction

Chromium (III) oxides are important materials in heterogeneous catalysis [1, 2], green pigments [3, 4], and industrial coatings for wear resistance and thermal protection [5–7]. They are also effective refractory materials due to their high melting temperature (~2300 °C) and oxidation resistance [8, 9]. Recently, there has been an interest in the development of chromium (III) oxide nanospheres to improve the sintering properties of these materials for refractory and ceramic applications. Nanosized powders present higher surface areas, potentially improving the sintering process by decreasing sintering temperatures and providing an increased density of sintered powders [8, 10, 11]. In addition, nanosphere chromium oxide particles are needed for utilization of chromium (III) oxide in transparent pigments [4, 12] and improved catalysts [1, 2]. To achieve this, strategies are needed to develop chromium (III) nanoparticles with controlled, narrow size distribution.

Several synthetic processing techniques for chromium III nanoparticles have been reported including precipitation–gelation reactions [13], sol–gel processes [8, 14], gas condensation [10], sonochemical reactions [15], laser-induced pyrolysis [16], forced hydrolysis [17, 18], mechanochemical processing [19], hydrothermal [20], and amorphous complexation methods using citric acid [21]. However, in most cases, irregular and ill-defined particle shapes were produced and particle agglomeration was obtained. In addition, industrial applications of some of these methods may be limited due to high cost and low yield. An economical, simple approach to creating chromium (III) oxide nanoparticles of controlled size, shape and high yields is needed. Precipitation from a Cr (III) salt solution has been shown as a cost-effective preparation method. This route can give high yields; however, difficulties in controlling nanoparticle size, purity, and agglomeration have been noted [13, 22–25].

This article reports using a modified approach utilizing homogenous urea-assisted precipitation with NaCl as a precipitating agent to produce high-purity chromic oxide nanoparticles of narrow size distribution in high yield. Under mild heating, urea decomposes, generating an

H. J. Gulley-Stahl · W. L. Schmidt · H. A. Bullen (✉)
Department of Chemistry, Northern Kentucky University, Highland Heights, KY 41099, USA
e-mail: bullenh1@nku.edu

increase in pH, which allows for homogeneous precipitation of numerous hydrated metal oxides [26–29]. The morphological size and shape, chemical composition, and crystallinity of the formed nanoparticles were evaluated. Results were compared to the previously reported method for urea-assisted hydrothermal synthesis of hydrated chromium oxide particles, which indicated Na_2SO_4 was necessary for particle precipitation and polyvinylpyrrolidone (PVP) was required to prevent particle agglomeration [22]. In addition, we report for the first time the use of attenuated total reflectance Fourier transform infrared spectroscopy (ATR-FTIR) to evaluate the effect of precipitating reagents on the surface reactivity of the chromium oxide nanoparticles to catechol. ATR-FTIR has been recently recognized as a powerful method for revealing the details of chemical reactions at solid-solution interface [30, 31], which have implications in a variety of fields including catalysis [32, 33], the dissolution of metal oxides [34], and corrosion of materials [35]. Metal oxide sol–gel films deposited on ATR crystals increase the sensitivity of ATR-FTIR measurements due to the large surface area that can concentrate analytes at the interface, permitting direct adsorbate/surface interactions to be monitored [36, 37].

Experimental

Materials

Chromium (III) nitrate nonahydrate ($Cr(NO_3)_3 \cdot 9H_2O$, Acros 99%) urea (Sigma–Aldrich, 99%) and NaCl (Fisher Chemical, 99%) were used as-received. All samples were prepared in DI water purified using a Milli-Q plus water purification system (Millipore, Bedford, MA). Additional reagents utilized in this work include Na_2SO_4 (Fisher Chemical, 99%) and polyvinyl pyrrolidone (PVP-360, Acros). A Cr_2O_3 powder standard (Sigma–Aldrich, 99%) was used for FTIR comparison.

Preparation of hydrated chromic oxide nanoparticles

Nanoparticles of narrow size distribution were prepared using a modified method reported previously [22, 24]. The particles were prepared by aging a 10 mL aliquot of 0.005 M chromium nitrate solution in the presence of NaCl (0.6 mol ratio Cl/Cr) and urea (0.02 mol/L). For aging, solutions were placed in a 15.0 mL pressure tube with a Teflon cap and placed in a preheated isotemp furnace at 100 °C for 24 h. After aging and cooling at room temperature for 6 h, the dark green particle suspension (yield 98%, based on chromium remaining in solution) was dialyzed for 48 h to remove excess ions from solution using regenerated cellulose dialysis tubing. It should be noted that the synthesis has been repeated on a larger scale (100 mL) with similar yields (90–97%). For comparison to previously reported methods [22], particles were also synthesized using Na_2SO_4 at a 0.6 mol ratio of sulfate/Cr instead of NaCl as described previously. The effect of adding PVP-360 (0.02 g/mL) on agglomeration of particles was also evaluated by forming nanoparticles with and without PVP present. As-formed nanoparticles were kept in aqueous solution or centrifuged and dried under vacuum for further analysis. For calcination, samples were heated for 1 h in a furnace at desired temperatures, and slowly cooled to room temperature inside the furnace.

Characterization

The size and morphology of the nanoparticles was examined using tapping mode with a Digital Instruments Dimension IV atomic force microscope (AFM) equipped with 125-μm silicon cantilevers with resonance frequencies between 150 and 200 kHz and typical scan rates of 1 Hz. For analysis, samples were drop cast from an aqueous solution onto silicon [111] substrates. Particle sizes were determined from cross-sectional height analysis of particles [38–40]. The statistical distribution of the particle size is a resultant of over 40 nanoparticle cross-sectional height profiles. Additionally, particles were analyzed with an IEF scanning electron microscope with Princeton Gamma-Tech (PGT) coupled energy dispersive X-ray spectrometer. The crystallinity of the nanoparticles was evaluated by powder X-ray diffraction with a Rigaku Ultima III powder X-ray diffractometer (XRD) using the Cu Kα radiation (40 kV, 44 mA). Data were collected over a 2θ range between 20 and 60° at scan rate of 0.1°/min. For FTIR analysis, the nanoparticles were mixed with KBr and analysis was conducted using a Nicolet NEXUS 670 FTIR equipped with a deuterated triglycine sulfate (DTGS) detector. Thermogravimetric analysis (TGA) of nanoparticles was conducted under high-purity N_2 using a TA Instruments, TGA 2050 thermogravimetric analyzer (30–1000 °C).

Surface reactivity

ATR-FTIR measurements were made using a horizontal attenuated total reflectance infrared (ATR-IR) attachment (Pike Technologies) with a 45° ZnSe crystal. The adsorption of catechol onto the nanoparticle films was evaluated. The films were formed by placing 400 μL samples of nanoparticle solution directly onto the ZnSe crystal, evaporating to dryness at room temperature (films formed about 1 μm thick according to AFM analysis). The particle films were rinsed with DI H_2O to remove loosely deposited particles. Spectra were taken at 64 scans and with a

resolution of 4 cm^{-1} using the ZnSe crystal with deposited nanoparticles as the background spectra. A sample (900 μL) of 0.01 M catecholate solution was directly placed onto the sol–gel and measurements were taken at 5-min intervals until equilibrium was established (~30 min). A spectral scan of water over the sol–gel was subtracted from the adsorbate spectral scan to minimize contributions of water to the spectra. For ease of spectral comparison, baselines were corrected without altering position or magnitude of peaks.

Results and discussion

Atomic force microscopy (AFM) was used to evaluate nanoparticle morphology. Figure 1a shows the AFM analysis of nanoparticles produced using NaCl as a precipitating agent. For comparison, the AFM analysis of particles produced with Na_2SO_4 as a precipitating agent [22] is also shown in Fig. 1b. In both syntheses, PVP was used as a surfactant, as it had been reported previously that the surfactant was necessary to control particle agglomeration [22]. For both NaCl and Na_2SO_4, the particles appeared to be randomly and homogeneously distributed. Under the experimental conditions chosen, the nanoparticles produced via Na_2SO_4 were comparable to those reported by Ocana [22] with an average size of 90 ± 15 nm (Fig. 1d). It can be clearly seen in Fig. 1a and c that nanoparticles produced using NaCl are significantly smaller than those produced from Na_2SO_4 and are more uniform in size and shape. The nanoparticles were found to be 3 ± 1 nm in dimension, according to cross-sectional height profiles. It should be noted that at this scale, tip convolution effects distorted the resolution in the lateral dimensions, as the dimensions of the particles are smaller than the radius of curvature of the AFM probe ($r \approx 15$ nm) [38, 39]. Similar to previous reports utilizing Na_2SO_4 [18, 22, 23], attempts to produce nanoparticles of narrow size distribution in the absence of Cl^- ions failed with gel-like, ill-defined systems produced. The Cl^- ion concentration was important in precipitation and controlling polydispersity of the nanoparticles. However, nanoparticle size was influenced by the concentration of Cr (III) ions in solution [22]. Larger particles were produced with increasing concentration of Cr^{3+} (keeping the Cl/Cr mole ratio constant), although sizes were not predictable. The reaction conditions described above (0.6 mol ratio of precipitating anion/Cr) produced nanoparticles of the most

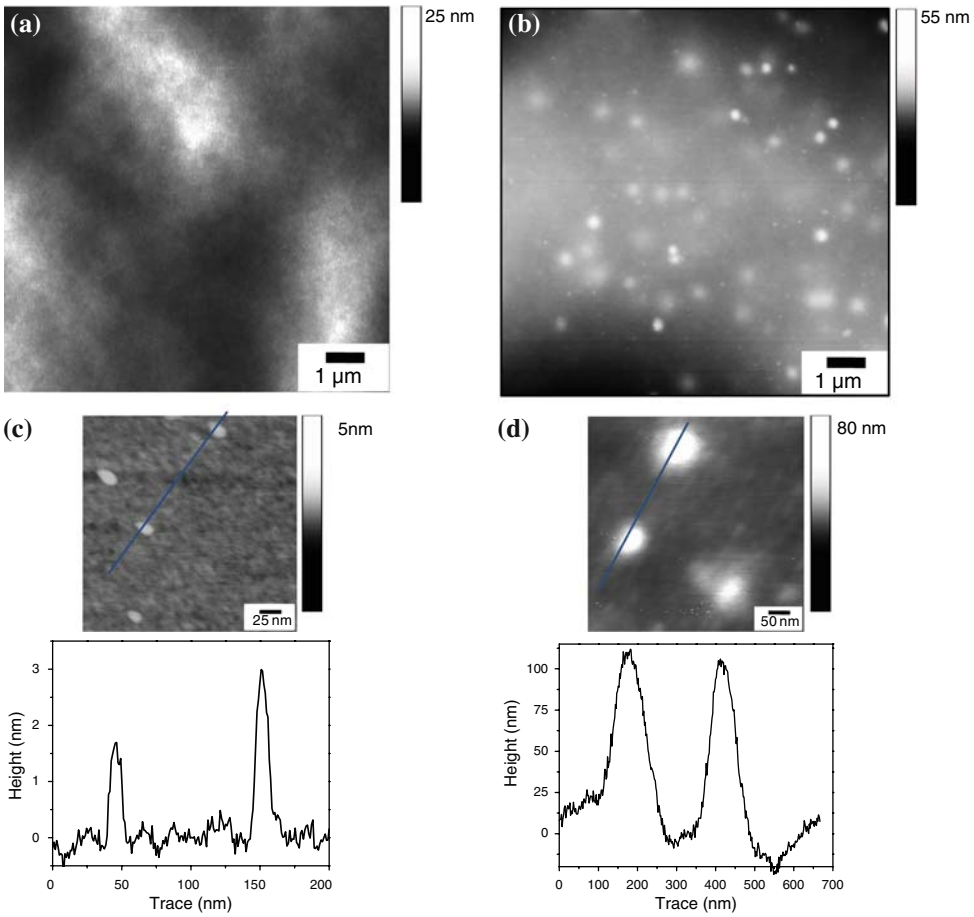

Fig. 1 AFM analysis, 10 × 10 μm^2, of nanoparticles produced using 0.2 g/mL of PVP and different precursors (**a**) NaCl and (**b**) Na_2SO_4. Representative cross-sectional height analyses of isolated particles produced using each precursor (**c**) NaCl and (**d**) Na_2SO_4 are also shown

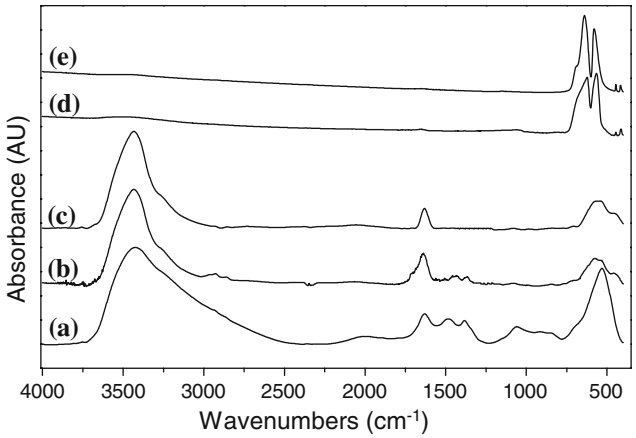

Fig. 2 FTIR analysis of nanoparticles produced under various precipitating agent and surfactant conductions: (**a**) Na_2SO_4 with PVP as-prepared, (**b**) NaCl with PVP as-prepared, (**c**) NaCl without PVP as-prepared, (**d**) NaCl without PVP, heated to 400 °C, and (**e**) Cr_2O_3 standard reference

uniform size and distribution. Therefore, subsequent analysis described here will focus on these reaction ratios.

The composition of the nanoparticles was evaluated using FTIR spectroscopy. The effects of precipitating agents (Na_2SO_4, NaCl), surfactant (PVP), and calcination on the composition are shown in Fig. 2. Particles produced by the previously reported method [22], utilizing Na_2SO_4 and PVP reagents, display an absorbance maximum at 540 cm^{-1}, which can be ascribed to Cr–O vibrations of chromium (III) hydroxide [25, 41], with bands at 1640 cm^{-1} and in the 3200–3600 cm^{-1} region indicating adsorbed water [15] (Fig. 2a). FTIR analysis also shows the presence of sulfate ($\sim$1100 cm^{-1}) [22, 25] and carbonate contaminates (1378 and 1482 cm^{-1}) [41]. The sulfate contaminates are attributed to the Na_2SO_4 precursor. Ocana [22] indicated that the carbonate contaminates were likely from the decomposition of urea [24]. Regardless of various washing methods [22, 24, 25], these contaminates could not be removed and remained present in the samples. The FTIR spectrum of nanoparticles synthesized with NaCl and PVP (Fig. 2b) is similar to that shown for the synthesis using Na_2SO_4 and PVP (Fig. 2a). However, two key differences can be noted. First, bands associated with sulfate contaminate are not present, as expected due to changing the precipitating ion. EDX analysis (Fig. 3) provides further verification and indicates that residual NaCl is not evident in the nanoparticles, unlike the sulfate ion (Fig. 3). Secondly, the absorbance maximum for Cr–O vibrations (Fig. 2b) was shifted to higher wavenumbers, $\sim$580 cm^{-1}, corresponding to the characteristic vibrational mode of symmetric CrO_6 octahedra of Cr_2O_3 [24]. These results suggest that the composition of as-prepared particles precipitated with NaCl is likely a hydrated Cr_2O_3 species, whereas Na_2SO_4

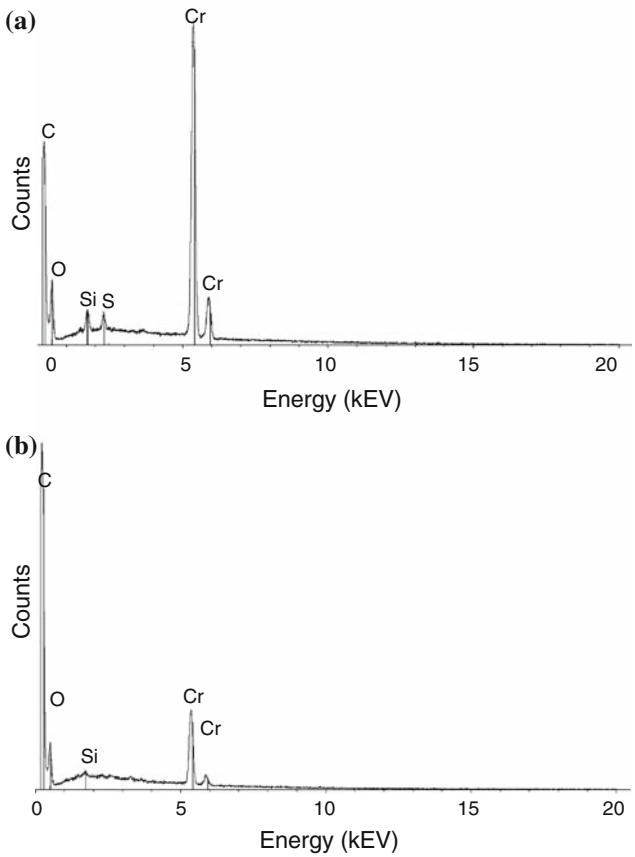

Fig. 3 EDX analysis of the Cr_2O_3 nanoparticles prepared using (**a**) Na_2SO_4 and (**b**) NaCl. The silicon and carbon peaks are due to the SEM substrate

precipitation creates primarily a chromium hydroxide species [23, 25, 41].

Utilization of NaCl instead of Na_2SO_4 as a precipitating reagent removed the precipitating agent contaminates from the nanoparticles; however, carbonate contaminates remained. Although carbonate contamination is likely from urea synthesis, prominent IR bands of PVP are also present within the 1378 and 1482 cm^{-1} region and could contribute to the contamination [42]. Therefore, in an attempt to further reduce contamination of as-prepared nanoparticles, synthesis of chromia nanoparticles was conducted utilizing NaCl as precipitating agent in the absence of PVP. FTIR analysis (Fig. 2c) confirms that contamination in the 1378–1482 cm^{-1} region has been significantly reduced. This modified synthesis not only removes contamination contributions from the surfactant, PVP, but also seems to minimize any carbonate contamination from urea decomposition. Any carbonate ions produced during synthesis are weakly bound to the surface of the nanoparticles and easily removed with additional dialysis, rather than incorporated into the nanoparticles themselves [22, 24, 25]. Furthermore, the chemical composition of the nanoparticles remained consistent with particles produced from NaCl

precipitation in the presence of PVP. Upon calcination at 400 °C, two well-resolved absorption bands at 570 and 638 cm^{-1} appear (Fig. 2d). These bands fall well within the range reported in the literature for bulk Cr_2O_3 [43] and are associated with Cr–O stretching modes in Cr_2O_3 due to various combination of Cr and O displacements in the lattice [44]. In addition, characteristic bands at 413 and 443 cm^{-1} appear and correlate with the bulk Cr_2O_3 standard (Fig. 2e).

Powder XRD was utilized to evaluate nanoparticle crystallinity. Figure 4a shows the characteristic X-ray diffraction pattern of as-prepared nanoparticles produced using NaCl in the absence of PVP. Although it has been reported that some crystalline metal oxides can be formed under controlled hydrolysis without calcination [27, 28], chromium oxide nanoparticles prepared here are amorphous. Results are similar for all synthetic conditions evaluated and are consistent with previously reported methods to synthesize Cr_2O_3 nanoparticles [10, 14–16, 20, 22, 24]. Annealing for 1 h at 400 °C produces the crystalline Cr_2O_3 phase, rhombohedral structure (space group R-3c (167), with lattice parameters $a = b = 4.9588$ Å and $c = 13.5942$ Å) [15, 45, 46], as shown in Fig. 4b. No other crystalline phases appear to be present. Thermal gravimetric analysis of the chromium oxide nanoparticles is shown in Fig. 5. Comparison to previously reported TGA/differential thermal analyses of Cr_2O_3 nanoparticles suggests that the crystalline phase transition starts around 300 °C [21, 22, 24], associated with no further weight loss. This is a lower temperature than previously reported for crystalline Cr_2O_3 nanoparticles and has been confirmed by XRD analysis [10, 14–16, 20, 22, 24]. The TG analysis also shows a broad decrease in weight starting at 100 °C characteristic of water and organic loss. The particles with

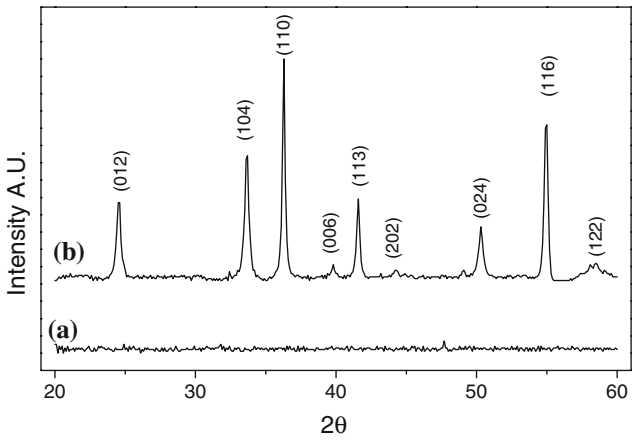

Fig. 4 X-ray diffraction patterns for chromium oxide nanoparticles: (**a**) as-prepared using NaCl as precipitating agent in the absence of PVP and (**b**) calcined at 400 °C. It should be noted that synthesis with PVP shows the same results

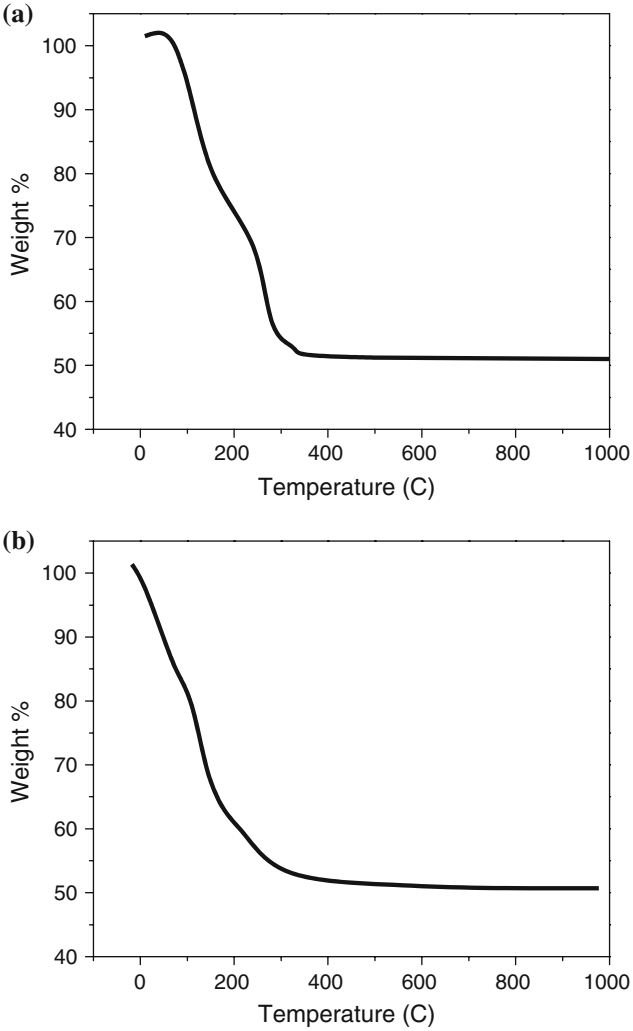

Fig. 5 TGA of as-prepared chromium oxide nanoparticles prepared by urea-assisted homogeneous precipitation with NaCl as a precipitating agent and (**a**) PVP, (**b**) no PVP

PVP show an additional loss in mass around 200–250 °C, which has been associated with carbonate ions [22] detected in the FTIR analysis. Overall there is only a small difference in overall weight loss, ~5%, which suggests that the carbonate contamination from PVP is not a large contribution to the overall original mass of the sample.

Ocana [22] had previously determined that PVP was necessary to prevent particle aggregation when using Na_2SO_4 as a precipitating agent. As shown in Fig. 5a and b, despite the absence of PVP, the nanoparticles produced using NaCl as a precipitating agent are quite uniform in size and shape. However, the morphology of the nanoparticles changed. Figure 6a clearly shows that the nanoparticles remain spherical-like in shape but are larger in dimension (85 ± 16 nm) compared to particles produced in the presence of PVP (3 ± 1 nm). Closer inspection (Fig. 6b) reveals the particles themselves are

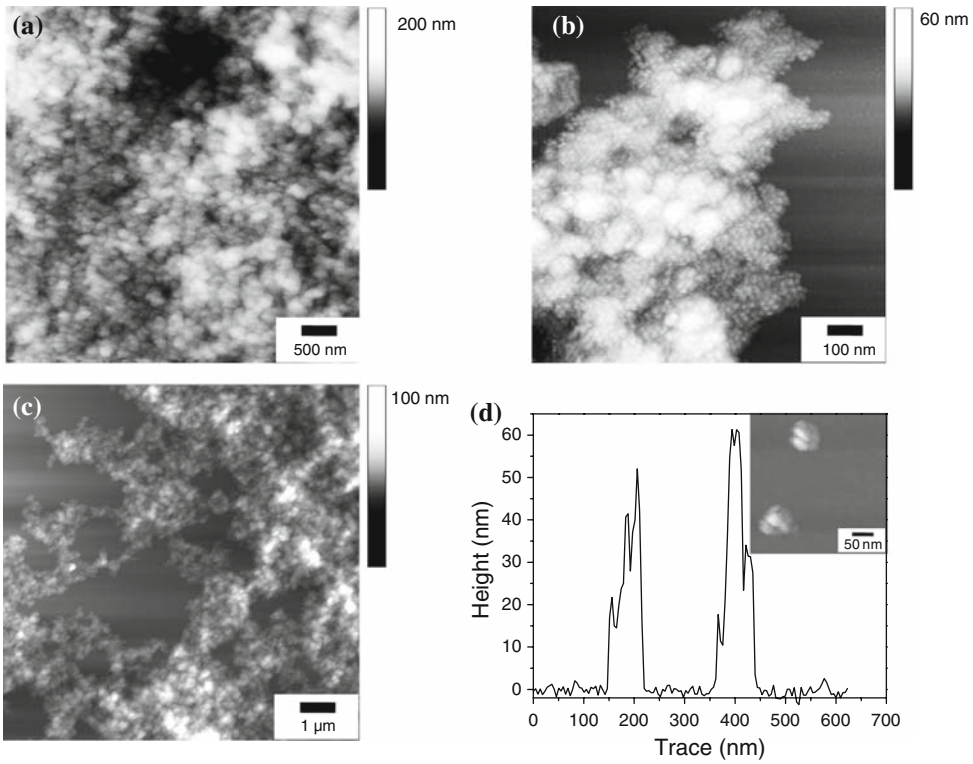

Fig. 6 AFM analysis of chromium oxide nanoparticles prepared by urea-assisted homogeneous precipitation with NaCl as a precipitating agent. As-prepared samples: (**a**) 5 × 5 μm^2 area and (**b**) 1 × 1 μm^2 area. After calcination at 400 °C: (**c**) 10 × 10 μm^2 and (**d**) representative cross-sectional height of particles

comprised of small subunits, ~10 nm diameter nanoparticles, which increase the surface area of the nanoparticles produced. This could prove useful in the application of these materials in catalysis applications. Overall the larger nanoparticles (85 ± 16 nm) are loosely aggregated and dispersion can be increased by sonication, without degradation of the particles and their subunits. After annealing to 400 °C, AFM analysis (Fig. 6c, d) indicates that the particles remain spherical-like, but decrease in size to ~65 ± 10 nm. XRD analysis using the Scherrer equation [47] for all diffraction peaks indicates the average crystallite size to be 20 nm. This correlates well with AFM analysis which reveals the 60 nm particles are still comprised of smaller subunits. The slight decrease in particle size is likely due to fusing of the void volume between the individual subunits of the nanoparticles upon calcination and crystallization. The nanoparticles do not appear to be strongly interconnected, but some aggregation of particles is evident.

Catechol was used to compare the surface reactivity of the chromium oxide nanoparticles created under different precipitating agent and surfactant conditions (Fig. 7). Catechol was chosen as model analyte as its derivatives are an important class of chemicals originating from both natural and anthropogenic sources, and it has shown to have a high affinity to metal oxide surfaces [36, 48, 49]. Adsorption of organic molecules onto mineral surfaces is generally thought to occur through either of two fundamental interactions: inner-sphere adsorption, in which the

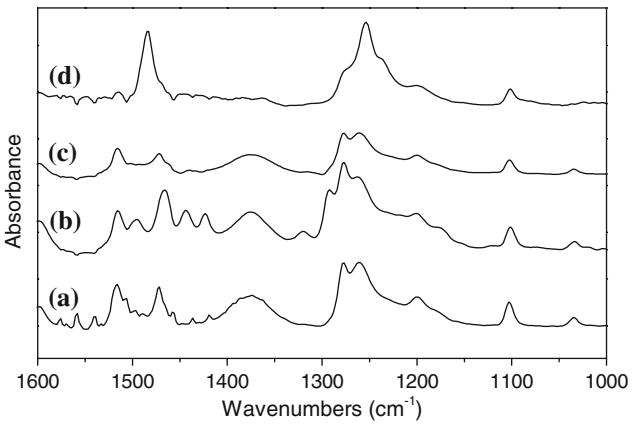

Fig. 7 ATR-FTIR analysis of (**a**) catechol (pH 7) and its interaction with chromium oxide nanoparticles prepared under different precipitating agent and surfactant conditions: (**b**) Na_2SO_4 with PVP, (**c**) NaCl with PVP, and (**d**) NaCl no PVP

organic anion forms a direct bond with the surface cation, or outer-sphere, where a direct anion-surface bond is formed [34]. Outer-sphere binding of organic anions generally gives rise to IR spectra that are similar to those of the anion in aqueous solution. The symmetry of anions is reduced when they adsorb in an inner sphere complex. Inner-sphere binding is often evident from shifting of bands, increased intensity of bands, and/or development of new bands, relative to the anion in aqueous solution [50, 51]. ATR-FTIR analysis suggests that catechol forms an outer-sphere complexation with the surface of the

nanoparticles prepared using Na_2SO_4 and NaCl in the presence of PVP (Fig. 7b, c). This is evident, as the spectrum is similar to that of catechol in solution, with little changes in spectral bands or intensities (Fig. 7a). However, catechol adsorbed on Cr_2O_3 hydrated nanoparticles prepared with NaCl in the absence of PVP (Fig. 7d) showed a five-fold increase in two main catechol bands, 1480 cm^{-1}, ν(–C=C–) and 1250 cm^{-1}, ν(C–O), which was independent of ionic strength. The splitting of the C–O stretching also disappeared, indicating a bidentate inner-sphere complex with Cr_2O_3 [36, 49]. These results clearly indicated that depending on the precipitation reagent, nanoparticle reactivity may vary.

Conclusions

In conclusion, a modified low-temperature method has been developed to produce weakly agglomerated spherical-like hydrated chromium oxide nanoparticles with narrow size distribution by aging chromium (III) nitrate in the presence of NaCl and urea at 100 °C. An advantage to this approach is that Cr_2O_3 nanoparticles of higher purity and composition, compared to those prepared with Na_2SO_4 and PVP, can be created under moderate conditions. Crystalline Cr_2O_3 nanoparticles can be produced with minimal agglomeration, by heating samples to 400 °C. Furthermore, ATR-FTIR results suggest that the reactivity of the Cr_2O_3 nanoparticles could potentially be tailored depending on the preparation method.

Acknowledgements This project was funded by the Merck Institute for Science Education, Kentucky NSF EPSCoR, Northern Kentucky University Center for Integrated Natural Science and Mathematics, NKU Greaves Endowment, and the NKU Research Foundation. The work was also supported in part by the National Science Foundation Instrument for Materials Research award (DMR-0526686) and Major Research Instrumentation award (EAR-0520921).

References

1. Kocon M, Michorczyk P, Ogonowski J (2005) Catal Lett 101:53
2. Wang S, Murata K, Hayakawa T, Hamakawa S (2000) Appl Catal A 196:1
3. Munoz R, Maso N, Julian B, Marquez F, Beltran H, Escribano P, Cordoncillo E (2004) J Eur Ceram Soc 24:2087
4. Brock T, Groteklaes M, Mischke P (2000) European coating handbook. Vincentz Verlag, Hanover, Germany
5. Cho B, Choi E, Chung S, Kim K, Kang T, Park C, Kim B (1999) Surf Sci 439:L799
6. Kitsunai H, Hokkirigawa K, Tsumaki N, Kato K (1991) Wear 151:279
7. Hsu C-H, Huang D-H, Ho W-Y, Huang L-T, Chang C-L (2006) Mater Sci Eng A 429:212
8. Kawabata A, Yoshinaka M, Hirota K, Yamaguchi O (1995) J Am Ceram Soc 78:2271
9. Kovarik O, Siegl J (2008) Strength Mater 40:79
10. Balachandran U, Siegel RW, Liao YX, Askew TR (1995) Nanostruct Mater 5:505
11. Ring T-A (1990) MRS Bull 15:34
12. Jiang L, Yusong W, Yubai P, Jingkun G (2006) J Non-Cryst Solids 352:2404
13. Kim D-W, Shin S-I, Lee JD, Oh S-G (2004) Mater Lett 58:1894
14. Chatterjee M, Siladitya B, Ganguli D (1995) Mater Lett 25:261
15. Arul Dhas N, Koltypin Y, Gendanken A (1997) Chem Mater 9:3159
16. Zhong ZC, Cheng RH, Bosley J, Dowben PA, Sellmyer DJ (2001) Appl Surf Sci 181:196
17. Morales JG, Carmona JG, Clemente RR, Muraviev D (2003) Langmuir 19:9110
18. Zettlemoyer AC, Siddiq M, Micale FJ (1978) J Colloid Interface Sci 66:173
19. Tsuzuki T, McCormick PG (2000) Acta Mater 48:2795
20. Xu H, Lou T, Li Y (2004) Inorg Chem Commun 7:666
21. Kim D-W, Oh S-G (2005) Mater Lett 59:976
22. Ocana M (2001) J Eur Ceram Soc 21:931
23. Demchak R, Matijevic E (1969) J Colloid Interface Sci 31:257
24. Music S, Maljkovic M, Popovic S, Trojko R (1999) Croat Chem Acta 72:789
25. Sprycha R, Matijevic E (1989) Langmuir 5:479
26. Subrt J, Stengl V, Bakardjieva S, Szatmary L (2006) Powder Technol 169:33
27. Soler-Illia G, Jobbagy M, Candal RJ, Regazzoni AE, Blesa MA (1998) J Dispers Sci Technol 19:207
28. Music S, Popovic S, Maljkovic M, Dragcevic D (2002) J Alloys Compd 347:324
29. Wang H, Fan Y, Shi G, Liu Z, Liu H, Bao X (2007) Catal Today 125:149
30. Hind AR, Bhargava SK, McKinnon A (2001) Adv Colloid Interface Sci 93:91
31. McQuillan AJ (2001) Adv Mater 13:1034
32. He R, Davda RR, Dumesic JA (2005) J Phys Chem B 109:2810
33. Burgi T, Bieri M (2004) J Phys Chem B 108:13364
34. O'Day PA (1999) Rev Geophys 37:249
35. Brown GE Jr, Henrich VE, Casey WH, Clark DL, Eggleston C, Felmy A, Goodman WA, Gratzel M, Maciel G, McCarthy MI, Nealson K, Sverjensky DA, Toney MF, Zachara JM (1999) Chem Rev 99:77
36. Connor PA, Dobson KD, McQuillan AJ (1995) Langmuir 11:4193
37. Rivera D, Harris JM (2001) Anal Chem 73:411
38. Yang D-Q, Xiong Y-O, Guo Y, Da D-A, Lu W-G (2000) J Mater Sci 36:263. doi:10.1023/A:1004894532155
39. Markiewicz P, Goh MC (1995) J Vac Sci Technol B 13:1115
40. Hosokawa M, Nogi K, Naito M, Yokoyama T (eds) (2007) Nanoparticle technology handbook. Elsevier, Oxford
41. Amonette JE, Rai D (1990) Clays Clay Miner 38:129
42. Bordoko Y, Humphrey SM, Tilley TD, Frei H, Somorjai GA (2007) J Phys Chem C 111:6288
43. Tabbal M, Kahwaji S, Christidis TC, Nsouli B, Zahraman K (2006) Thin Solid Films 515:1976
44. Brown DA, Cunningham D, Glass WK (1968) Spectrochim Acta A 24:965
45. Banobre-Lopez M, Vazquez-Vazquez C, Rivas J, Lopez-Quintela MA (2003) Nanotechnology 14:318
46. Finger LW, Hazen RM (1980) J Appl Phys 51:5362
47. Patterson AL (1939) Phys Rev 56:978
48. Vasudevan D, Stone AT (1996) Environ Sci Technol 30:1604
49. Araujo PZ, Morando PJ, Blesa MA (2005) Langmuir 21:3470
50. Duckworth OW, Martin ST (2001) Geochim Cosmochim Acta 65:4289
51. Johnson SB, Yoon TH, Kocar BD, Brown GE Jr (2004) Langmuir 20:4996